

Data-Driven Discovery of High-Performance Heterobilayer Transition Metal Dichalcogenide-Based Sliding Ferroelectrics

Xian Wang, Peng Wang, Xiaoqing Liu, Xuesen Wang, Yunpeng Lu,* and Lei Shen*



Cite This: <https://doi.org/10.1021/acsmi.4c19017>



Read Online

ACCESS |

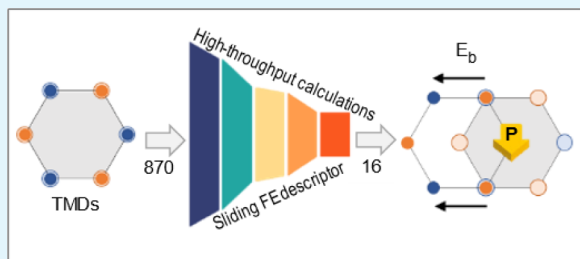
Metrics & More

Article Recommendations

Supporting Information

ABSTRACT: The development of efficient sliding ferroelectric (FE) materials is crucial for advancing next-generation low-power nanodevices. Currently, most efforts focus on homobilayer two-dimensional materials, except for the experimentally reported heterobilayer sliding FE, MoS₂/WS₂. Here, we first screened 870 transition metal dichalcogenide (TMD) bilayer heterostructures derived from experimentally characterized monolayer TMDs and systematically investigated their sliding ferroelectric behavior across various stacking configurations using high-throughput calculations. On the basis of the generated data, we developed an efficient descriptor, named the amplitude of Allen electronegativity difference ($\Delta\chi_m$), for identifying van der Waals heterobilayers with sliding FE properties. Finally, 16 semiconducting TMD heterobilayers are identified as exhibiting interlayer sliding FE alongside low switching barriers (<21 meV/f.u.), with 10 outperforming the experimental MoS₂/WS₂ system, showing the largest out-of-plane polarization (OPP) values up to 10 times higher than MoS₂/WS₂. These materials exhibit favorable band gaps (0.60–1.80 eV) using the HSE06 method, making them suitable for sliding FE applications. Our findings reveal that polarization switching in these heterobilayers is strongly influenced by the interplay of stacking patterns, material electronegativity, charge transfer, and electronic structures. This study provides a robust framework for designing novel sliding ferroelectric materials and offers a theoretical basis for future experimental research.

KEYWORDS: *sliding ferroelectricity, high-throughput calculations, material electronegativity, out-of-plane polarization, sliding energy barrier*



INTRODUCTION

Ferroelectric materials play a pivotal role in a wide range of technological applications, such as nonvolatile memory devices and microelectromechanical systems (MEMS).^{1–3} While conventional ferroelectric materials exhibit excellent ferroelectric properties, their three-dimensional structures present formidable challenges in meeting the demands for miniaturization and low-power consumption in advanced modern devices.^{4–6} In contrast, two-dimensional (2D) materials, with their unique structural, electronic, and physical properties, have emerged as highly promising candidates for the next generation of ferroelectric materials.^{7–9} Among the novel phenomena recently observed in 2D materials, sliding ferroelectricity (FE) has attracted considerable attention due to its potential to enable low-power, high-efficiency electronic devices.^{10–12} Unlike conventional ferroelectric mechanisms that rely on ionic displacement for polarization switching, sliding FE is driven by the reversible translational sliding of one monolayer relative to the other via van der Waals (vdW) interactions, unlocking new opportunities for ferroelectric applications in nanoelectronics. The sliding is the key to switching the polarization. Thus, the layered 2D materials with weak vdW

interactions offer the best platform for this new ferroelectric system.^{13–15}

Transition metal dichalcogenides (TMDs), known for their unique structural and electronic properties, ease of synthesis, scalability, and recently demonstrated sliding ferroelectric behavior in experimental systems, have emerged as promising candidates for exploring sliding FE.^{16–18} Sliding FE has been reported in several TMD-based homobilayers, including MX₂ compounds (M = Mo, W, and X = S, Se, and Te) both theoretically and experimentally.^{17,19,20} However, the ferroelectric response in homobilayers is typically weak, such as only about 0.5 pC/m of sliding FE in homobilayer MoX₂ (X = S, Se, and Te).¹⁷ This is largely because of the limited asymmetry between the similar layers, which inherently restricts polarization switching.²¹ This limitation presents critical challenges for practical applications, particularly in

Received: November 2, 2024

Revised: December 31, 2024

Accepted: January 8, 2025

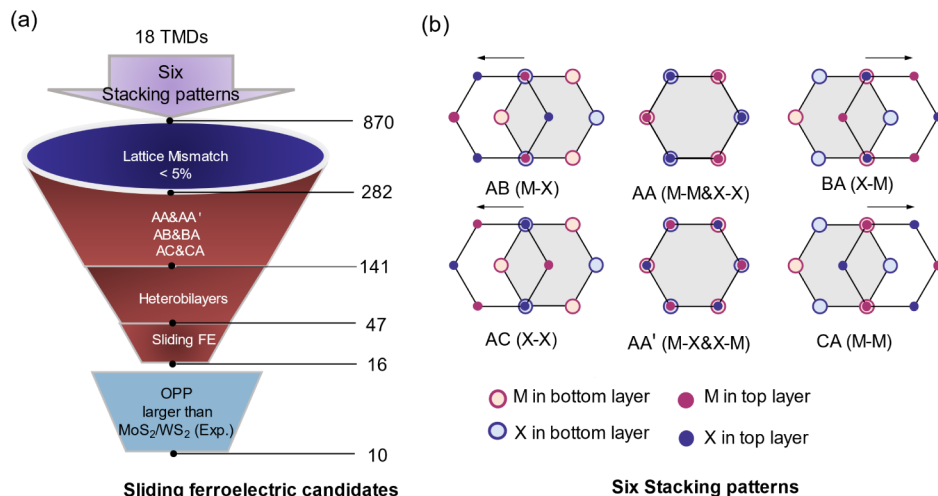


Figure 1. Overall workflow for identifying TMD heterobilayer candidates with strong out-of-plane ferroelectric polarization (OPP). (a) Based on 18 TMD monolayers, the screening process involved constructing heterobilayers with a lattice mismatch of less than 5%, resulting in 47×6 bilayer heterostructures. From these, 16 sliding ferroelectric candidates were identified, 10 exhibiting larger OPP compared to the well-known MoS_2/WS_2 system. (b) Six main stacking patterns of the bilayer structure.

devices such as nonvolatile memory and sensors, where robust and stable polarization switching is crucial.^{22–24}

In response to these constraints, research has shifted toward the study of heterobilayers composed of distinct TMD layers, which are held together by vdW interactions.^{25–27} These heterobilayers introduce novel interfacial effects that offer greater tunability of ferroelectric response and energy barriers required for polarization switching, making them more suitable for technological applications.^{28–30} A landmark study by Rogée et al.²⁹ provided the first experimental observation of out-of-plane FE in an untwisted, commensurate, and epitaxial MoS_2/WS_2 heterobilayer, synthesized via a scalable one-step chemical vapor deposition process. This groundbreaking discovery has paved the way for further exploration of sliding FE in vdW heterobilayers, underscoring their potential for advanced device applications. Despite this progress, the study of sliding FE behavior in heterobilayers remains relatively scarce, highlighting the need for further identification of more heterobilayer sliding ferroelectrics. Moreover, more data are needed to investigate the underlying mechanisms and optimize the strategies to fully harness their potential in nanoelectronics and other applications.

In this study, we first screened 870 TMD bilayer heterostructures based on monolayer TMDs and systematically investigated their sliding ferroelectric behavior across various stacking configurations. We introduce the amplitude of the Allen material electronegativity difference ($\Delta\chi_m$) between monolayers as a reliable predictor of switching polarization.³¹ It is found that $\Delta\chi_m$ values below 0.15 strongly indicate sliding ferroelectric behavior. Among the heterobilayers, 16 semiconducting candidates were identified with FE properties alongside low switching barriers, with 10 candidates having 1 order of magnitude higher out-of-plane polarization (OPP) than the well-known MoS_2/WS_2 system.²⁹ Additionally, favorable band gaps of these 10 candidates suggest their broad application potential. The relationships between polarization switching, energy barriers, interlayer coupling, and charge transfer (CT) highlight the critical role of constituent element electronegativity, interlayer spacing, lattice parameters, and interlayer stacking patterns in determining polarization behavior. This study provides a robust framework for

predicting sliding ferroelectricity and offers valuable insights for the rational design of novel ferroelectric materials, establishing a foundation for future experimental and theoretical advancements in the field.

METHODS

All first-principles calculations were conducted using the Vienna Ab Initio Simulation Package (VASP) within the density functional theory (DFT) framework.^{32,33} The projector-augmented wave (PAW) method was utilized to accurately describe both core and valence electrons.³⁴ The exchange-correlation interactions were treated using the Perdew–Burke–Ernzerhof (PBE) functional within the generalized gradient approximation (GGA).³⁵ A plane-wave energy cutoff of 600 eV was selected to ensure the convergence of the total energies. Electronic minimization was performed with a strict convergence criterion of 10^{-6} eV, guaranteeing precise determination of the electronic ground state. Ionic relaxation was carried out with a force tolerance of 0.005 eV/Å, ensuring the accurate optimization of atomic structures in the bilayers. To prevent artificial interactions between periodically repeated bilayer structures, a vacuum region of at least 20 Å was introduced, effectively isolating each bilayer. The Brillouin zone was sampled using a Γ -centered $15 \times 15 \times 1$ Monkhorst–Pack k-point mesh.³⁶ Given the significant role of vdW interactions in layered materials, the D3 Grimme method was employed, accurately accounting for dispersive forces between layers, particularly in sliding ferroelectric materials.³⁷ Ferroelectric polarizations, with consideration of dipole correction, were evaluated using the Berry-phase method.^{38,39} We validated our method using previously reported TMD homobilayer sliding ferroelectrics, including MoS_2 , MoSe_2 , and MoTe_2 . The predicted values of 0.45–0.54 pC/m are in good agreement with the measured value of 0.53 pC/m.¹⁷ Additionally, the energy barriers for various kinetic processes were determined using the climbing image nudged elastic band (CI-NEB) method,⁴⁰ which allows for precise identification of transition states and energy barriers along reaction pathways, providing valuable insights into the switching behavior of polarization states. The electronic structure was evaluated using the HSE06 hybrid functional, which performs well in band gap predictions.^{41,42}

RESULTS AND DISCUSSION

The nonmagnetic monolayer TMDs are denoted as MX_2 ($\text{M} = \text{Ti}, \text{Zr}, \text{Hf}, \text{Cr}, \text{Mo}, \text{and W}$, and $\text{X} = \text{S}, \text{Se}, \text{and Te}$), which have been experimentally synthesized.^{43,44} In a monolayer, an M

atom is sandwiched between two X atom layers, forming a trigonal prismatic geometry in which each M atom is coordinated by six X atoms positioned above and below the M atom. As shown in **Table S1**, the lattice constants of these materials range from 3.03 Å (CrS₂) to 3.92 Å (ZrTe₂). Their electronic structures were calculated using the HSE06 hybrid functional method, obtaining key parameters such as band gaps, gap types, conduction band minimum (CBM), and valence band maximum (VBM), as depicted in **Figures S1–S3** and **Table S1**. These compounds exhibit a range of band gap values from 0.87 to 2.36 eV, with good semiconducting properties observed across all materials, highlighting their potential for electronic and optoelectronic applications.^{10,45} Notably, larger band gaps above 2 eV are observed in materials such as MoS₂ and WX₂ (X = S, Se, and Te), while smaller band gaps around 1 eV are seen in compounds like MTe₂ (M = Ti, Zr, Hf, and Cr). Materials such as MX₂ (M = Ti, Zr, and Hf, and X = S, Se, and Te) predominantly exhibit indirect band gaps, while MX₂ (M = Cr, Mo, and W, and X = S, Se, and Te) has direct band gaps. The variation in band gaps across these materials suggests the potential for tuning electronic properties by combining them into heterobilayers. Our results provide meaningful insights into the electronic properties of TMD semiconductors, offering valuable information for the design of next-generation electronic and optoelectronic devices based on vdW heterobilayers.

Further, 870 bilayer heterostructures were constructed by applying lattice rotation and translation based on 18 monolayer TMDs,^{46–48} denoted as M_TX_T/M_BX_B. Here, M_TX_T/M_BX_B refers to the top (T) and bottom (B) layers, respectively (**Figure 1a**). Upon stacking, six primary configurations were considered, as illustrated in **Figure 1b**: AA, AA', AB, BA, AC, and CA. The AA configuration represents the simplest arrangement, where each atom in the top layer is positioned directly above its counterpart in the bottom layer. In the AA' configuration, the X_T/M_T atom of the top layer aligns directly above the X_B/M_B atom in the bottom layer. In the AC/CA configurations, the X_T/M_T atom of the top layer is positioned directly over the X_B/M_B atom of the bottom layer, while the M_T/X_T atom of the top layer is placed above the center of a hexagon in the bottom layer. Conversely, in the AB/BA configurations, the X_T/M_T atom of the top layer is positioned over the center of a hexagon in the bottom layer, with the M_T/X_T atom aligned directly above the X_B/M_B atom of the bottom layer. AB and BA stackings can be achieved through mutual in-plane sliding, as can AC and CA stackings. Additionally, the AA stacking can be derived by performing a 180° in-plane rotation of the AA' configuration. For clarity, the AA and AA' configurations are grouped as the AA(AA') pair, AB and BA as the AB(BA) pair, and AC and CA as the AC(CA) pair.

Considering the lattice mismatch between different materials, we identified 282 bilayer heterostructures (**Figure 1a**), ensuring that the mismatch remained below 5%. Since AA(AA'), AB(BA), and AC(CA) stacking configurations are treated as pairs during sliding/twisting, these strategic arrangements resulted in 141 (282/2) distinct bilayer heterostructure pairs and 47 (141/3) independent heterobilayers with different monolayers, offering a comprehensive framework for studying ferroelectric behaviors, as illustrated in **Figure 1**. Through high-throughput calculations on the 47 candidates, 16 heterobilayers were identified with AB and BA stackings possessing sliding FE characteristics, as detailed in

Table S2. These heterobilayers include TiSe₂/ZrS₂, TiSe₂/HfS₂, TiSe₂/HfSe₂, TiTe₂/ZrTe₂, TiTe₂/HfTe₂, ZrS₂/ZrSe₂, ZrS₂/HfS₂, ZrSe₂/HfSe₂, ZrTe₂/HfTe₂, HfS₂/HfSe₂, CrS₂/MoS₂, CrSe₂/MoSe₂, CrTe₂/MoTe₂, MoS₂/WS₂, MoSe₂/WSe₂, and MoSe₂/WS₂. To evaluate the stability of these heterobilayers, the formation energy was calculated, defined as the energy difference between the heterobilayers and their corresponding monolayers. As depicted in **Figure S4**, the formation energy for all heterobilayers is negative, signifying that they are energetically favorable. The consistent negative formation energies across all heterobilayers indicate that these bilayer systems are likely to be synthesized in experiments. However, the synthesis of heterobilayers presents additional challenges, including lattice mismatch, interfacial defects, and the complexity of achieving precise stacking orders.^{30,49} Overcoming these obstacles through advanced synthesis techniques, interface engineering strategies, and phase engineering is crucial for advancing the practical applications of sliding FE materials. Actually, some of the heterobilayers, such as MoS₂/WS₂, MoSe₂/WSe₂, and WS₂/MoSe₂ have been experimentally reported.^{25,26,28}

The performance of the sliding FE in TMD heterobilayers is influenced by two crucial factors. First, the interlayer sliding, which drives the strength and direction of polarization switching, is highly dependent on the variation in the interlayer interaction strengths across different TMD combinations. Second, the energy barrier for polarization switching plays a crucial role in determining the practical viability of a sliding FE. **Figure 2a** shows the downward and upward out-of-plane polarization (OPP_{up}, OPP_{down}) values for all 16 heterobilayers. MoS₂/WS₂ is selected as a reference material because its sliding FE properties have been reported in the experiment.²⁹

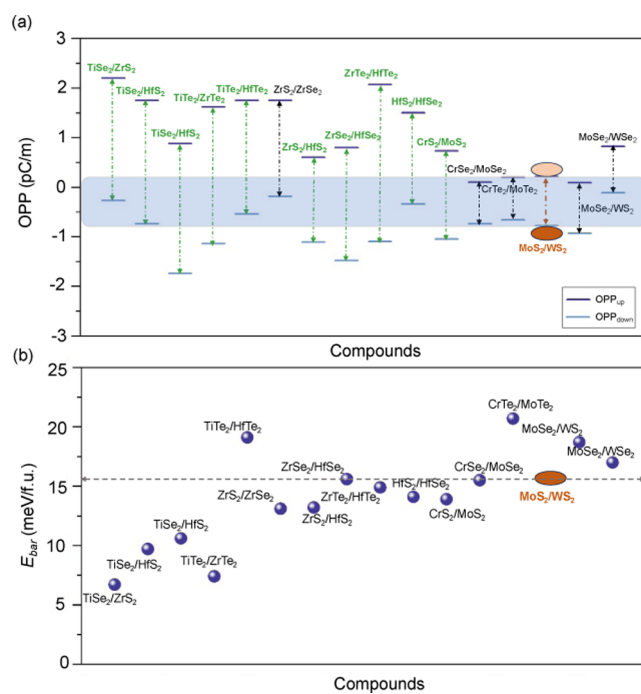


Figure 2. (a) The upward and downward out-of-plane polarization (OPP_{up} and OPP_{down} in pC/m) values and (b) energy barrier (E_{bar}, in meV/f.u.) for AB and BA stackings. The experimental sliding FE MoS₂/WS₂ heterobilayer highlighted in orange is used as a reference. The 10 heterobilayers with the OPP larger than MoS₂/WS₂ are highlighted in green.

OPP_{down} and OPP_{up} values for MoS₂/WS₂ are determined to be -0.78 and 0.21 pC/m, respectively. From the heterobilayers screened for higher OPP values, 10 candidates are identified, including TiSe₂/ZrS₂, TiSe₂/HfS₂, TiSe₂/HfSe₂, TiTe₂/ZrTe₂, TiTe₂/HfTe₂, ZrS₂/HfS₂, ZrSe₂/HfSe₂, ZrTe₂/HfTe₂, HfS₂/HfSe₂, and CrS₂/MoS₂. As reported in a previous study, Zhang et al.³⁰ demonstrated the modulation of polarization in sliding ferroelectrics by introducing intrinsic electric fields, which are regulated through the electronegativity differences among chalcogens, leading to improved polarization, achieving a maximum value of 1.18 pC/m, representing a 65% enhancement compared to conventional TMD bilayers MX₂ (M = Mo and W, and X = S, Se, and Te). Interestingly, these heterobilayers in our work exhibit large OPP values up to 10 times higher than MoS₂/WS₂. Notably, four heterobilayers exhibit OPP values surpassing the largest OPP of MoS₂/WS₂, which are TiSe₂/HfSe₂ (-1.74, 0.88 pC/m), TiTe₂/ZrTe₂ (1.14, -1.62 pC/m), ZrSe₂/HfSe₂ (-1.48, 0.80 pC/m), and ZrTe₂/HfTe₂ (-1.10, 2.07 pC/m). For instance, the OPP_{down} and OPP_{up} values for ZrTe₂/HfTe₂ are approximately 1.5 and 10 times greater than those of the MoS₂/WS₂ system, respectively. Additionally, TiSe₂/ZrS₂ and ZrTe₂/HfTe₂ exhibit OPP values exceeding 2.00 pC/m in one direction. These results underscore the potential for enhanced sliding ferroelectric applications. Some heterobilayers display notable polarization asymmetry, characterized by large OPP values in one direction and much smaller values in the opposite direction. For instance, the OPP values are -0.18 and 1.75 pC/m for ZrS₂/ZrSe₂, -0.74 and 0.10 pC/m for CrSe₂/MoSe₂, -0.93 and 0.09 pC/m for MoSe₂/WS₂, and -0.11 and 0.82 pC/m for MoSe₂/WSe₂. These results highlight the diversity in polarization behavior across different heterobilayers, suggesting that the intrinsic properties of each material pair play a crucial role in determining the polarization characteristics.

Moreover, achieving optimal energy barriers between downward and upward OPP is crucial for sliding ferroelectricity in real device applications.^{7,18} A low energy barrier in the experiment may lead to unintended polarization switching and increased leakage currents, while a high energy barrier slows the switching process, reducing device performance. Therefore, optimizing the energy barrier to balance a fast response with minimal leakage is a critical challenge in advancing sliding FE for practical applications. Thus, the feasibility of polarization inversion was assessed by evaluating the switching barriers, which were further calculated using the CI-NEB method, providing accurate insights into transition states and energy profiles.⁴⁰ The sliding ferroelectric switching pathways of studied systems are provided in Figures S5–S8. As illustrated in Figure 2b, all 16 heterobilayers exhibit relatively low switching barriers between the OPP_{down} and the OPP_{up}, with most falling below 21 meV/f.u., with the highest at 20.7 meV/f.u., and the lowest at 6.7 meV/f.u. The characteristic heterobilayer MoS₂/WS₂ has an energy barrier of 15.7 meV/f.u., which has been identified experimentally.²⁹ These heterobilayers exhibit remarkably low sliding switching barriers compared to other reported 2D ferroelectric materials.^{51–54} For example, Cheng et al.⁵¹ predicted γ-XOOH (X = Al, Ga, and In) monolayers with ferroelastic and ferroelectric properties, showing switching barriers of 76–106 meV/f.u. Similarly, Gao and Chelikowsky⁵² demonstrated intrinsic ferroelectricity in As₂X₃ (X = S, Se, and Te) with barriers of 200–380 meV/f.u. In contrast, TMD-based sliding FE heterobilayers achieve

much lower barriers (<21 meV/f.u.), highlighting their potential for energy-efficient applications. Notably, TiSe₂/HfSe₂, TiTe₂/ZrTe₂, ZrSe₂/HfSe₂, and ZrTe₂/HfTe₂ show energy barriers of 10.6, 7.4, 15.6, and 14.9 meV/f.u., respectively. These four materials exhibit larger OPP_{down/up} values while maintaining lower energy barriers compared to MoS₂/WS₂. For comparison, the energy barrier for sliding FE in vdW-layered yttrium-doped γ-InSe has been experimentally determined to be approximately 30 meV/f.u.⁵⁵ The relatively low energy barriers observed in these heterobilayers suggest efficient FE switching, making all of them promising candidates for next-generation ferroelectric applications in which both performance and stability are crucial.

The switching of the polarization direction during the sliding process, a critical feature of sliding FE, is primarily dictated by the direction of CT. High-throughput computational analysis has demonstrated that only a small subset of heterobilayers exhibit sliding FE, characterized by polarization switching. While interlayer CT is frequently observed in heterobilayers, it does not necessarily lead to sliding FE. Understanding the mechanisms and factors that govern polarization switching in heterobilayers is essential for advancing the development of sliding ferroelectric materials. CT between materials is strongly influenced by the relative electronegativities of the constituent cations and anions. However, in heterobilayers, which are composed of multiple elements, the complexity of the interlayer interactions makes it challenging to explain CT dynamics solely based on the electronegativity of individual ions. Therefore, a more comprehensive approach is necessary to fully elucidate the behavior of the sliding FE in these systems. Here, we developed a method to estimate material electronegativity, termed the Allen material electronegativity, derived from the Allen element electronegativity (χ_e).³¹ The Allen element electronegativity is primarily based on the average energy of the valence electrons in free atoms. The rationale for using the Allen electronegativity lies in the fundamental principle that energy transfer, including that of valence electrons, occurs from higher to lower energy levels. As shown in Table S1, the material electronegativity (χ_m) parameters for 18 monolayer TMD materials were calculated by³¹

$$\chi_m = \frac{(n_{sm}\epsilon_{sm} + n_{dm}\epsilon_{dm}) + 2(n_{sx}\epsilon_{sx} + n_{px}\epsilon_{px})}{(n_{sm} + n_{dm}) + 2(n_{sx} + n_{px})} \quad (1)$$

where $\epsilon_{sm, dm, sx, px}$ represent the one-electron energies of the s and d electrons in the transition metal atom, and the s and p electrons in the chalcogen atom, respectively. The corresponding numbers of valence electrons, $n_{sm, dm, sx, px}$ refer to the s and d electrons in the transition metal atom and the s and p electrons in the chalcogen atom. The one-electron energy values can be directly obtained from spectroscopic data, which are readily available for most elements, while the number of s, p, and d electrons can be determined through Bader charge analysis. The general trend observed for χ_m is that materials with higher χ_m values have a stronger tendency to attract electrons, indicating their greater electronegativity. A larger difference in χ_m is expected to result in a more distinct charge transfer, with electrons moving from the material with lower χ_m to the one with higher χ_m . For sliding ferroelectrics, an excessively strong CT presents challenges to reversing its direction via interlayer sliding due to the presence of a large interfacial electric field in heterobilayer systems.^{31,50} Conversely, when the χ_m difference

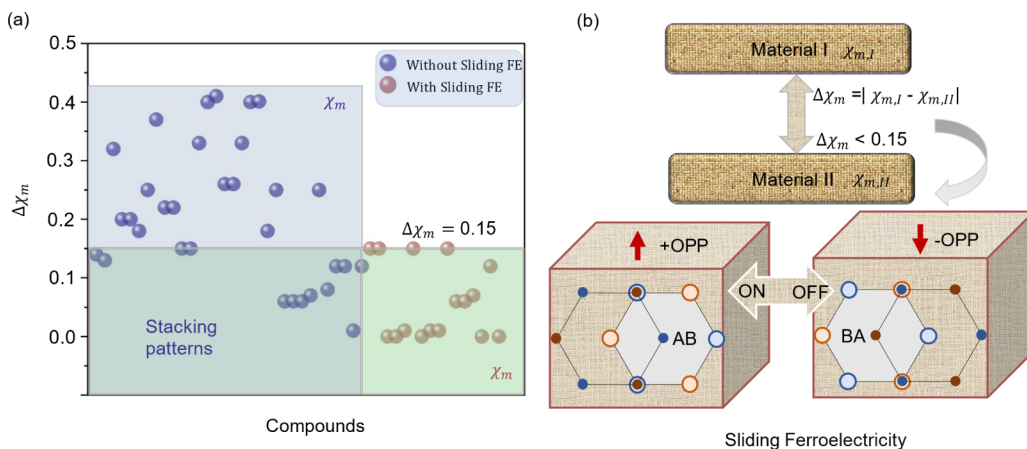


Figure 3. (a) The absolute difference in material electronegativity ($\Delta\chi_m$) between two 2D materials, denoted as Material I and Material II, where $\Delta\chi_m = |\chi(I) - \chi(II)|$. (b) Schematic diagram illustrating the determination of $\Delta\chi_m$ and the polarization switching in a sliding FE.

is too small, the direction of electron transfer becomes ambiguous and susceptible to external perturbations. In sliding ferroelectric applications, CT within a heterobilayer typically follows a specific direction and must be altered by external stimuli to achieve polarization switching. Therefore, selecting an appropriate material electronegativity difference is crucial for accurately predicting the potential for polarization switching.

To address this, we propose the use of the absolute difference in material electronegativity $\Delta\chi_m$ between two 2D materials, denoted as Material I and Material II, where $\Delta\chi_m = |\chi(I) - \chi(II)|$, as a descriptor for predicting the possibility of polarization switching in sliding FE heterobilayers. As shown in Figure 3, the $\Delta\chi_m$ magnitudes of 47 independently constructed TMD heterobilayers were systematically analyzed. The results reveal a distinct trend: when $\Delta\chi_m$ exceeds 0.15, none of the heterobilayers exhibited sliding FE, whereas for $\Delta\chi_m$ values below 0.15, a cluster of sliding ferroelectric samples was observed. NEB calculations validate this approach, showing that TMD-based heterobilayers with $\Delta\chi_m < 0.15$ exhibit very low energy barriers (<21 meV/f.u.). This finding underscores the remarkable dependence of sliding FE on the relative electronegativity of the constituent materials. However, the emergence of sliding FE is not solely dictated by material electronegativity but also by the spatial arrangement and stacking configuration of the layers. Consequently, even in cases where $\Delta\chi_m$ is less than 0.15, certain heterobilayers do not exhibit sliding FE, highlighting the complexity of interlayer interactions and the critical influence of geometric factors on the ferroelectric behavior. Thus, additional computational studies are necessary to accurately predict polarization in certain cases following our selection criteria. The findings indicate that sliding FE is absent in the majority of heterobilayers. The proposed $\Delta\chi_m$ metric offers a valuable preliminary criterion for identifying materials with potential sliding FE, thereby serving as a practical guide to streamline experimental efforts.

OPP, defined as the dipole moment per unit area, was analyzed in terms of electronic and ionic contributions, as presented in Tables S5 and S6. The contributions were found to be opposite, with the electronic component dominating in the AB stacking and the ionic component prevailing in the BA stacking, indicating a strong dependence on the stacking configuration. Further, an in-depth investigation into the

mechanisms was conducted by examining differential charge densities (DCD) at the interface in 16 heterobilayers with OPP_{down} and OPP_{up} stacking configurations. DCD, a measure of charge redistribution, represents the difference between the charge densities of the heterobilayer, the top layer, and the bottom layer. Additionally, plane-averaged charge density plots along the out-of-plane direction were employed to qualitatively visualize CT within the systems. As shown in Figures 4 and S9–S11, these results clearly demonstrate charge redistribution between the top and bottom layers, indicated by regions of electron accumulation (red areas) and electron depletion (green areas). Their line profiles highlight the presence of electric polarization at the interface, with the switching of the polarization direction through lateral sliding. All of the materials indicate that the interfacial chalcogens play a more crucial role in contributing to polarization than the center metals. The variation in electron depletion at the chalcogen interfaces induces a net interlayer charge transfer. This charge transfer arises from stacking-induced asymmetry, where the bottom M atom aligns directly above the top X atom, while the bottom X atom is located above a hollow site. This asymmetric stacking configuration results in enhanced electron depletion from the bottom X atoms compared with the top X atoms, leading to a downward polarization. Conversely, in the case where the top M atom is aligned directly above the bottom X atom and the top X atom is positioned over a hollow site, the stacking asymmetry causes greater electron depletion from the top X atoms relative to that from the bottom X atoms, resulting in a downward polarization. The transition metals Ti, Zr, and Hf tend to enhance the strength of polarization compared with Cr, Mo, and W.

Subsequently, three distinct scenarios are systematically analyzed: the same M atom with varying X atoms, different M atoms with the same X atom, and both M and X atoms being different. Here, representative examples include ZrS₂/ZrSe₂, TiTe₂/ZrTe₂, and TiSe₂/ZrS₂. In the case of ZrS₂/ZrSe₂, the OPP_{down} and the OPP_{up} values are -0.18 and 1.75 pC/m, respectively, with an interlayer distance of 3.74 Å and a surface area of approximately 11.36 Å². The interlayer distance is defined as the vertical distance between the nearest neighboring atoms in the upper and lower layers. The corresponding charge transfers are 0.004 and 0.007 au. This structure features the same transition metal Zr element but different chalcogens, S and Se. Notably, S has a slightly higher

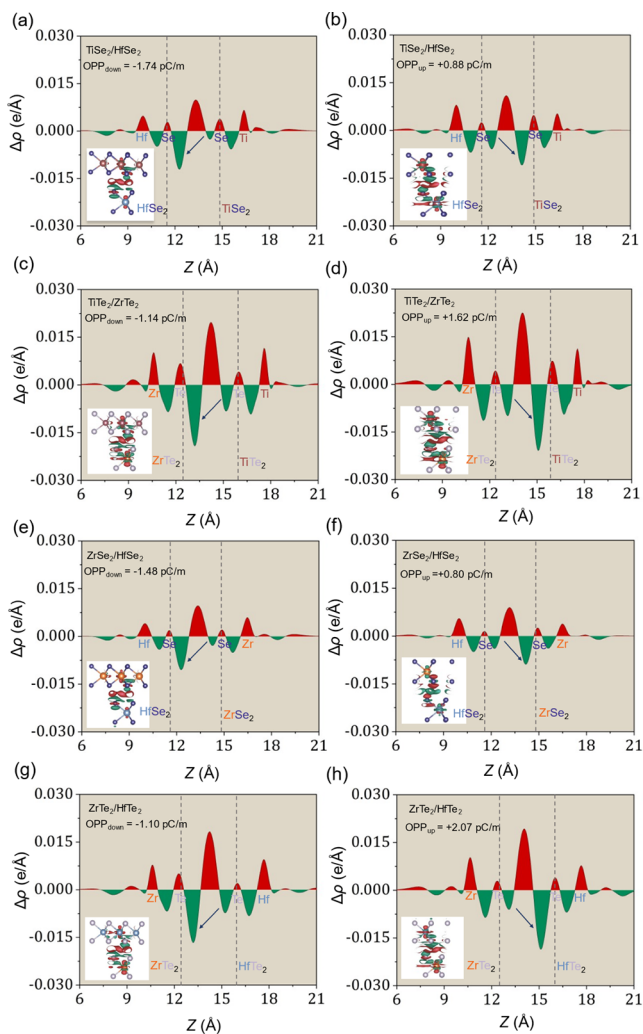


Figure 4. Differential charge densities and their line profiles along the z direction for (a, b) $\text{TiSe}_2/\text{HfSe}_2$, (c, d) $\text{TiTe}_2/\text{ZrTe}_2$, (e, f) $\text{ZrSe}_2/\text{HfSe}_2$, and (g, h) $\text{ZrTe}_2/\text{HfTe}_2$ with two OPP_{down} (AB) and OPP_{up} (BA) stacking configurations. The isosurface value is $0.0001 \text{ e}/\text{\AA}^3$. The red regions indicate charge accumulation, while the green regions represent charge depletion.

electronegativity (2.5) compared to Se (2.4). The electronegativity of ZrS_2 is 2.34, while that of ZrSe_2 is 2.20, and the

difference is about 0.14. The value of the OPP_{up} is approximately 10 times greater than that of the OPP_{down} . The remarkable differences in OPP values suggest that the stacking pattern exerts a more dominant influence on the OPP than the electronegativity of chalcogens. For $\text{TiTe}_2/\text{ZrTe}_2$, the OPP_{down} and the OPP_{up} are -1.14 and 1.62 pC/m , with an interlayer distance of approximately 4.00 \AA and a surface area of 12.66 \AA^2 . The charge transfers are 0.016 and 0.017 au , respectively. In this system, the chalcogen Te remains the same, while the transition metals Ti and Zr differ. Ti has a slightly higher electronegativity (1.5) compared to Zr (1.4). The electronegativity values of TiTe_2 and ZrTe_2 are both about 1.97. The moderate variation in the OPP values highlights the greater influence of the stacking arrangement on the OPP compared to the electronegativity of the transition metals. In the case of $\text{TiSe}_2/\text{ZrS}_2$, the OPP_{down} and OPP_{up} are -0.27 and 2.20 pC/m , respectively, with interlayer distances of 3.70 \AA and a surface area of 10.76 \AA^2 . The charge transfers are approximately 0.007 and 0.014 au , respectively. The electronegativity of TiSe_2 is approximately 2.19, while that of ZrS_2 is around 2.34, with a difference of about 0.15. The OPP_{up} is roughly 10 times greater than OPP_{down} , once again indicating that the stacking arrangement and material electronegativity have a substantial impact on both the strength and direction of OPP. Comparing the different heterobilayers, the interlayer CT, surface area, and interlayer spacing also exhibit a notable influence on the intensity of OPP (see Figure 4). These findings suggest that the strength and direction of the OPP in these layered heterobilayers are strongly influenced by the interplay between the electronegativity of the constituent elements, the magnitude of charge transfer, interlayer spacing, lattice parameters, and stacking patterns. These interdependencies emphasize the critical role of the atomic composition and structural factors in determining the polarization properties. In practical experiments, interfacial roughness, temperature, and electric fields significantly impact the stability and ferroelectric performance.^{56–58} For example, Zhang et al.⁵⁶ revealed that interface roughness enhances remnant polarization in $\text{Hf}_{0.5}\text{Zr}_{0.5}\text{O}_2$ films but increases leakage current and degrades endurance, highlighting optimization needs for advanced ferroelectric memory. Thus, optimizing the synthesis to improve interfacial smoothness, minimize thermal vibrations, and ensure uniform electric fields is essential for achieving reliable and high-performance FE materials.

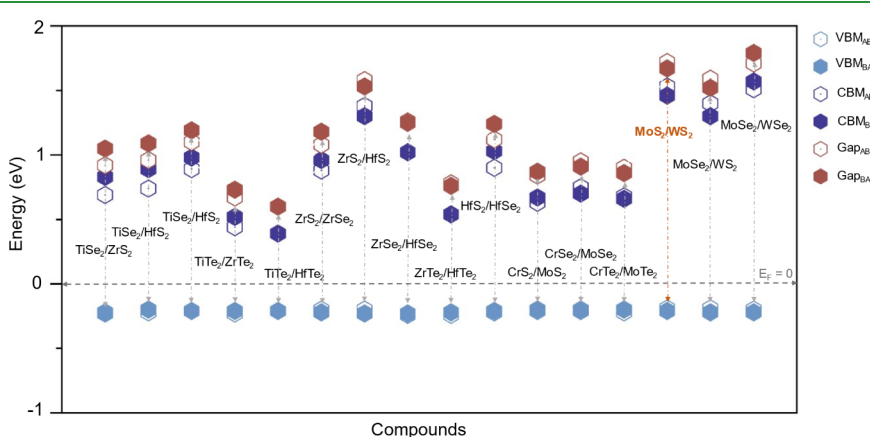


Figure 5. Valence band maximum (VBM), conduction band minimum (CBM), and band gaps of 16 TMD heterobilayers with the OPP_{down} (AB) and the OPP_{up} (BA) stacking configurations were calculated using the HSE06 method. The Fermi energy (E_F) was shifted to zero for reference.

Sliding ferroelectric materials possess the distinctive ability to reverse ferroelectric polarization through interlayer sliding, positioning them as promising candidates for next-generation electronic devices.^{12,59,60} However, the presence of an appropriate band gap is essential for the design of energy-efficient devices or possibly being integrated into current Si-based devices.⁴⁵ Therefore, the band structures of 16 heterobilayers with AB (OPP_{down}) and BA (OPP_{up}) stacking configurations were analyzed by using the HSE06 hybrid functional method. Crucial parameters such as band gaps, gap types, CBM, and VBM were predicted, revealing similar values for OPP_{down} and OPP_{up} configurations as shown in Figure 5 and Tables S2 and S3. All heterobilayers exhibit semiconducting behavior, with band gaps ranging from 0.60 to 1.79 eV, where the possible applications are described in the Supporting Information. Specifically, TiTe₂/ZrTe₂, TiTe₂/HfTe₂, CrS₂/MoS₂, CrSe₂/MoSe₂, and CrTe₂/MoTe₂ possess band gaps between 0.60 and 0.91 eV, while TiSe₂/ZrS₂, TiSe₂/HfS₂, ZrS₂/ZrSe₂, ZrSe₂/HfSe₂, and HfS₂/HfSe₂ show band gaps from 1.00 to 1.25 eV. Additionally, ZrS₂/HfS₂, MoS₂/WS₂, MoSe₂/WS₂, and MoSe₂/WSe₂ exhibit band gaps ranging from 1.52 to 1.79 eV. Among these, CrSe₂/MoSe₂, CrTe₂/MoTe₂, MoSe₂/WS₂, and MoSe₂/WSe₂ feature direct band gaps, while the rest display indirect band gaps.

Furthermore, the detailed band structures of these heterobilayers are illustrated in Figures 6, S12, and S13. For systems such as TiSe₂/ZrS₂, TiSe₂/HfS₂, TiSe₂/HfSe₂, TiTe₂/ZrTe₂, TiTe₂/HfTe₂, ZrS₂/HfS₂, ZrSe₂/HfSe₂, ZrTe₂/HfTe₂, and HfS₂/HfSe₂, it is observed that the valence band (VB) is primarily governed by the p-orbitals of chalcogen atoms, whereas the conduction band (CB) is largely dictated by the d-orbitals of transition metals. Generally, CT primarily occurs between the p-orbitals of chalcogen atoms and the d-orbitals of transition metal atoms. Specifically, in the OPP_{down} configuration of TiSe₂/HfSe₂, Hf significantly influences the CBM, whereas in the OPP_{up} configuration, the contributions from Ti and Hf become more comparable, with neither metal dominating. A similar trend is seen in TiTe₂/ZrTe₂, where Zr plays a more prominent role in the CBM for the OPP_{down} configuration, but for the OPP_{up}, the contributions of Ti and Zr become more balanced. In the case of ZrSe₂/HfSe₂, for the OPP_{down} configuration, Hf dominates the CBM, but when the stacking is in the OPP_{up} configuration, the Zr contribution becomes more pronounced, effectively shifting the balance of influence. A comparable behavior is observed in ZrTe₂/HfTe₂, where Zr plays a crucial role in the CBM for the OPP_{down}, while Hf assumes dominance in the OPP_{up} configuration. A similar trend is observed across the other six analogous structures (Figure S12). This finding shows that the change in metal contributions with stacking configuration emphasizes the impact of stacking on the VBM, CBM, and OPP.

For the CrS₂/MoS₂, CrSe₂/MoSe₂, CrTe₂/MoTe₂, MoS₂/WS₂, MoSe₂/WS₂, and MoSe₂/WSe₂ heterobilayers, both the VBM and CBM are predominantly controlled by the transition metals, as shown in Figure S13. For instance, in MoS₂/WS₂, Mo dictates the CBM, while W primarily contributes to the VBM in both stacking configurations. Similar trends are noted in MoSe₂/WS₂. In CrS₂/MoS₂, CrSe₂/MoSe₂, and CrTe₂/MoTe₂, the CBM is largely influenced by Cr, while Mo governs the VBM, regardless of the stacking configuration OPP_{down} or OPP_{up}. A slight deviation occurs in MoSe₂/WSe₂, where W dominates the CBM while Mo retains control over the VBM, again for both the OPP_{down} and the OPP_{up}.

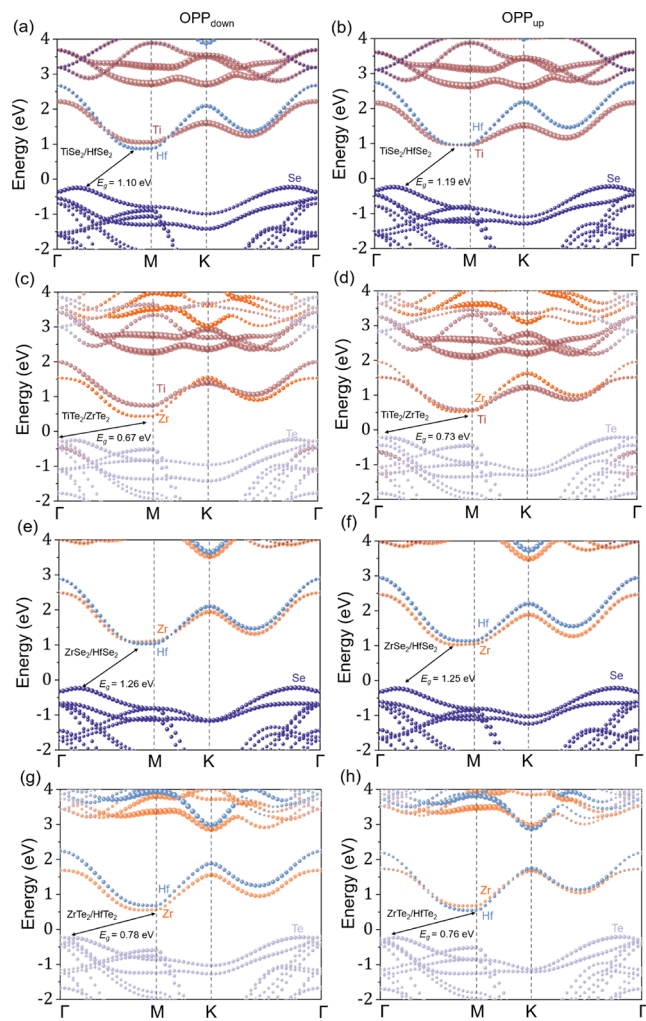


Figure 6. Band structure of (a, b) TeSe₂/HfSe₂, (c, d) TiTe₂/ZrTe₂, (e, f) ZrSe₂/HfSe₂, and (g, h) ZrTe₂/HfTe₂ heterobilayers with OPP_{down} (AB) and OPP_{up} (BA) stacking configurations at the HSE06 level.

configurations. The shift in elemental dominance between the CBM and VBM based on stacking configuration highlights the critical role of structural arrangement in tuning the electronic properties of these materials.

Our band structure analysis reveals that, despite identical elemental composition, different stacking configurations result in notable variations in the contributions of elements to the conduction and valence bands. In certain cases, this may lead to pronounced differences in the OPP between AB and BA stackings. Based on the analysis, the distinct band structures of MX₂ (M = Ti, Zr, and Hf, and X = S, Se, and Te) and MX₂ (M = Cr, Mo, and W, and X = S, Se, and Te) reveal notable differences in polarization properties, with the former exhibiting larger OPP compared to the latter. This difference is likely due to the dominant contributions to the VBM and CBM, where chalcogen atoms dominate in the former, while transition metals dominate in the latter. These findings highlight the critical influence of stacking configurations and material composition on the electronic and polarization behaviors of layered heterostructures.

Studies have demonstrated that heterobilayer TMDs exhibit high-performance sliding FE, characterized by strong OPP and low sliding switching energy barriers, alongside bandgap

properties that are well-suited for semiconductor applications, such as $\text{TiSe}_2/\text{HfSe}_2$, $\text{TiTe}_2/\text{ZrTe}_2$, $\text{ZrSe}_2/\text{HfSe}_2$, and $\text{ZrTe}_2/\text{HfTe}_2$. Experimental synthesis has already been successfully achieved for MoS_2/WS_2 heterostructures,²⁹ and other TMD-based sliding ferroelectrics with superior performance also show promise for experimental validation. Benefiting from their unique properties, TMD-based ferroelectrics hold significant potential for applications in future nanoelectronics, energy harvesting, and sensing technologies.^{16–18} Despite the immense potential of TMDs in sliding FE, challenges remain for large-scale applications.^{30,49} Moreover, the successful integration of sliding ferroelectric materials into existing semiconductor platforms necessitates compatibility with current technologies, while their commercialization critically depends on cost reduction through the development of efficient and scalable fabrication methods, such as large-scale liquid-phase deposition, coupled with advanced performance optimization strategies.^{7,10,61} As research progresses, TMD-based sliding ferroelectrics are expected to demonstrate tremendous potential in emerging fields such as quantum computing and artificial intelligence, further driving innovation and technological development.^{62,63}

CONCLUSIONS

Using a data-driven approach, we proposed the amplitude of the Allen material electronegativity difference ($\Delta\chi_m$) between the monolayers as an efficient predictor for polarization switching potential, finding that $\Delta\chi_m$ values below 0.15 indicate a strong possibility of sliding FE behavior in heterobilayers. Through high-throughput DFT calculations, we identified 16 TMD-based heterobilayers with sliding FE properties, 10 of which exhibit larger out-of-plane polarization than the experimentally reported MoS_2/WS_2 , along with low sliding energy barriers (<21 meV/f.u.). These high-performance candidates include $\text{TiSe}_2/\text{ZrS}_2$, $\text{TiSe}_2/\text{HfS}_2$, $\text{TiSe}_2/\text{HfSe}_2$, $\text{TiTe}_2/\text{ZrTe}_2$, $\text{TiTe}_2/\text{HfTe}_2$, $\text{ZrS}_2/\text{HfS}_2$, $\text{ZrTe}_2/\text{HfTe}_2$, $\text{HfS}_2/\text{HfSe}_2$, and $\text{CrS}_2/\text{MoS}_2$, with the largest OPP value being approximately 10 times greater than that of MoS_2/WS_2 . As predicted by the HSE06 hybrid functional, these heterobilayers exhibit favorable band gaps ranging from 0.60 to 1.80 eV. Moreover, a comprehensive physical analysis reveals that OPP is strongly correlated with the material electronegativity, charge transfer, stacking patterns, interlayer spacing, and lattice parameters. Our studies provide a foundational framework for predicting the presence of sliding FE in TMD-based heterobilayers, offering valuable insights for the rational design of novel sliding ferroelectrics. The comprehensive analysis presented here not only informs future experimental research but also lays the theoretical groundwork for the development of next-generation ferroelectrics.

ASSOCIATED CONTENT

Supporting Information

The Supporting Information is available free of charge at <https://pubs.acs.org/doi/10.1021/acsami.4c19017>.

Detailed calculations of lattice parameters, valence and conduction band edges, Fermi energy, band gaps, polarizations, and their contributions for monolayer TMDs and their heterostructures with sliding FE; analysis of ferroelectric switching pathways, energy barriers, and differential charge densities for these

heterostructures; insights into electronic properties using HSE06-level methods ([PDF](#))

AUTHOR INFORMATION

Corresponding Authors

Yunpeng Lu – School of Chemistry, Chemical Engineering and Biotechnology, Nanyang Technological University, Singapore 637371, Singapore; [orcid.org/0000-0003-2493-7853](#); Email: yplu@ntu.edu.sg

Lei Shen – Department of Mechanical Engineering, National University of Singapore, Singapore 117575, Singapore; [orcid.org/0000-0001-6198-5753](#); Email: shenlei@nus.edu.sg

Authors

Xian Wang – School of Chemistry, Chemical Engineering and Biotechnology, Nanyang Technological University, Singapore 637371, Singapore; [orcid.org/0000-0002-4017-8036](#)

Peng Wang – College of Electronic and Information Engineering, Shandong University of Science and Technology, Qingdao 266590, China

Xiaojing Liu – Department of Mechanical Engineering, National University of Singapore, Singapore 117575, Singapore

Xuesen Wang – Department of Physics, National University of Singapore, Singapore 117551, Singapore

Complete contact information is available at:
<https://pubs.acs.org/10.1021/acsami.4c19017>

Author Contributions

LYP, SL, and WX initiated this work. WX completed the models, codes, computations, and the first draft. WX, WP, LXQ, and WXS analyzed the data. WX, LYP, WXS, and SL reviewed the whole manuscript.

Notes

The authors declare no competing financial interest.

ACKNOWLEDGMENTS

SL acknowledges the financial support from Singapore MOE Tier 1 (No. A-8001194-00-00) and Singapore MOE Tier 2 (No. A-8001872-00-00). WX and SL acknowledge the financial support from Singapore MOE Tier 1 (No. 23-0450-A0001). WX and LYP acknowledge the financial support from Singapore MOE Tier 1 under its Academic Research Fund Tier 1 RG82/22.

REFERENCES

- (1) Scott, J. F. Applications of Modern Ferroelectrics. *Science* **2007**, 315, 954.
- (2) Choi, K. J.; Biegalski, M.; Li, Y. L.; Sharan, A.; Schubert, J.; Uecker, R.; Reiche, P.; Chen, Y. B.; Pan, X. Q.; Gopalan, V. Enhancement of Ferroelectricity in Strained BaTiO_3 Thin Films. *Science* **2004**, 306, 1005.
- (3) Jia, X.; Guo, R.; Tay, B. K.; Yan, X. Flexible Ferroelectric Devices: Status and Applications. *Adv. Funct. Mater.* **2022**, 32, 2205933.
- (4) Junquera, J.; Ghosez, P. Thickness for Ferroelectricity in Perovskite Ultrathin Films. *Nature* **2003**, 422, 506.
- (5) Sai, N.; Kolpak, A. M.; Rappe, A. M. Ferroelectricity in Ultrathin Perovskite Films. *Phys. Rev. B* **2005**, 72 (2), 020101.
- (6) Martin, L. W.; Rappe, A. M. Thin-Film Ferroelectric Materials and Their Applications. *Nat. Rev. Mater.* **2017**, 2 (2), 16087.

- (7) Fox, C.; Mao, Y.; Zhang, X.; Wang, Y.; Xiao, J. Stacking Order Engineering of Two-Dimensional Materials and Device Applications. *Chem. Rev.* **2024**, *124* (4), 1862–1898.
- (8) Wang, C.; You, L.; Cobden, D.; Wang, J. Towards Two-Dimensional Van Der Waals Ferroelectrics. *Nat. Mater.* **2023**, *22*, 542.
- (9) Wu, J.; Chen, H.-Y.; Yang, N.; Cao, J.; Yan, X.; Liu, F.; Sun, Q.; Ling, X.; Guo, J.; Wang, H. High Tunneling Electroresistance in a Ferroelectric Van Der Waals Heterojunction via Giant Barrier Height Modulation. *Nat. Electron.* **2020**, *3*, 466.
- (10) Wu, M.; Li, L. Sliding Ferroelectricity in 2D Van Der Waals Materials: Related Physics and Future Opportunities. *Proc. Natl. Acad. Sci. U.S.A.* **2021**, *118* (50), No. e2115703118.
- (11) Li, S.; Wang, F.; Wang, Y.; Yang, J.; Wang, X.; Zhan, X.; He, J.; Wang, Z. Van Der Waals Ferroelectrics: Theories, Materials, and Device Applications. *Adv. Mater.* **2024**, *36* (22), 2301472.
- (12) Vizner Stern, M.; Waschitz, Y.; Cao, W.; Nevo, I.; Watanabe, K.; Taniguchi, T.; Sela, E.; Urbakh, M.; Hod, O.; Ben Shalom, M. Interfacial Ferroelectricity by Van Der Waals Sliding. *Science* **2021**, *372*, 1462.
- (13) Zhang, D.; Schoenherr, P.; Sharma, P.; Seidel, J. Ferroelectric Order in Van Der Waals Layered Materials. *Nat. Rev. Mater.* **2023**, *8*, 25.
- (14) Man, P.; Huang, L.; Zhao, J.; Ly, T. H. Ferroic Phases in Two-Dimensional Materials. *Chem. Rev.* **2023**, *123*, 10990.
- (15) Li, T.; Wu, Y.; Yu, G.; Li, S.; Ren, Y.; Liu, Y.; Liu, J.; Feng, H.; Deng, Y.; Chen, M.; Zhang, Z. Realization of Sextuple Polarization States and Interstate Switching in Antiferroelectric CuInP₂S₆. *Nat. Commun.* **2024**, *15* (1), 2653.
- (16) Lin, Z.; Si, C.; Duan, S.; Wang, C.; Duan, W. Dichalcogenides Controlled by Electronic Ferroelectricity. *Phys. Rev. B* **2019**, *100*, 155408.
- (17) Wang, X.; Yasuda, K.; Zhang, Y.; Liu, S.; Watanabe, K.; Taniguchi, T.; Hone, J.; Fu, L.; Jarillo-Herrero, P. Interfacial Ferroelectricity in Rhombohedral-Stacked Bilayer Transition Metal Dichalcogenides. *Nat. Nanotechnol.* **2022**, *17*, 367.
- (18) Meng, P.; Wu, Y.; Bian, R.; Pan, E.; Dong, B.; Zhao, X.; Chen, J.; Wu, L.; Sun, Y.; Fu, Q. Sliding Induced Multiple Polarization States in Two-Dimensional Ferroelectrics. *Nat. Commun.* **2022**, *13*, 7696.
- (19) Li, L.; Wu, M. Binary Compound Bilayer and Multilayer with Vertical Polarizations: Two-Dimensional Ferroelectrics, Multiferroics, and Nanogenerators. *ACS Nano* **2017**, *11*, 6382.
- (20) Yang, Q.; Wu, M.; Li, J. Origin of Two-Dimensional Vertical Ferroelectricity in WTe₂ Bilayer and Multilayer. *J. Phys. Chem. Lett.* **2018**, *9*, 7160.
- (21) Naumis, G. G.; Herrera, S. A.; Poudel, S. P.; Nakamura, H.; Barraza-Lopez, S. J. Mechanical, Electronic, Optical, Piezoelectric and Ferroic Properties of Strained Graphene and Other Strained Monolayers and Multilayers: An Update. *Rep. Prog. Phys.* **2024**, *87*, 016502.
- (22) Han, S.-T.; Zhou, Y.; Roy, V. A. L. Towards the Development of Flexible Non-Volatile Memories. *Adv. Mater.* **2013**, *25*, 5425.
- (23) Ahn, E. C.; Wong, H.-S. P.; Pop, E. Carbon Nanomaterials for Non-Volatile Memories. *Nat. Rev. Mater.* **2018**, *3* (3), 18009.
- (24) Baek, S. H.; Jang, H. W.; Folkman, C. M.; Li, Y. L.; Winchester, B.; Zhang, J. X.; He, Q.; Chu, Y. H.; Nelson, C. T.; Rzchowski, M. S. Ferroelastic Switching for Nanoscale Non-Volatile Magnetoelectric Devices. *Nat. Mater.* **2010**, *9*, 309.
- (25) Zhang, C.; Chuu, C.-P.; Ren, X.; Li, M.-Y.; Li, L.-J.; Jin, C.; Chou, M.-Y.; Shih, C.-K. Interlayer Couplings, Moiré Patterns, and 2D Electronic Superlattices in MoS₂/WSe₂ Hetero-Bilayers. *Sci. Adv.* **2017**, *3* (1), No. e1601459.
- (26) Sebait, R.; Rosati, R.; Yun, S. J.; Dhakal, K. P.; Brem, S.; Biswas, C.; Puretzky, A.; Malic, E.; Lee, Y. H. Sequential Order Dependent Dark-Exciton Modulation in Bi-Layered TMD Heterostructure. *Nat. Commun.* **2023**, *14* (1), 5548.
- (27) Regan, E. C.; Wang, D.; Paik, E. Y.; Zeng, Y.; Zhang, L.; Zhu, J.; MacDonald, A. H.; Deng, H.; Wang, F. Emerging Exciton Physics in Transition Metal Dichalcogenide Heterobilayers. *Nat. Rev. Mater.* **2022**, *7*, 778.
- (28) Hsu, W.-T.; Lu, L.-S.; Wu, P.-H.; Lee, M.-H.; Chen, P.-J.; Wu, P.-Y.; Chou, Y.-C.; Jeng, H.-T.; Li, L.-J.; Chu, M.-W.; Chang, W.-H. Negative Circular Polarization Emissions from WSe₂/MoSe₂ Commensurate Heterobilayers. *Nat. Commun.* **2018**, *9* (1), 1356.
- (29) Rogée, L.; Wang, L.; Zhang, Y.; Cai, S.; Wang, P.; Chhowalla, M.; Ji, W.; Lau, S. P. Ferroelectricity in Untwisted Heterobilayers of Transition Metal Dichalcogenides. *Science* **2022**, *376*, 973.
- (30) Wilson, N. P.; Yao, W.; Shan, J.; Xu, X. Excitons and Emergent Quantum Phenomena in Stacked 2D Semiconductors. *Nature* **2021**, *599*, 383.
- (31) Liu, X.; Zhao, Y.-M.; Zhang, X.; Wang, L.; Shen, J.; Zhou, M.; Shen, L. Data-Driven Discovery of Transition Metal Dichalcogenide-Based Z-Scheme Photocatalytic Heterostructures. *ACS Catal.* **2023**, *13*, 9936.
- (32) Kresse, G.; Furthmüller, J. Efficient Iterative Schemes for Ab Initio Total-Energy Calculations Using a Plane-Wave Basis Set. *Phys. Rev. B* **1996**, *54*, 11169.
- (33) Kresse, G.; Furthmüller, J. Efficiency of Ab-Initio Total Energy Calculations for Metals and Semiconductors Using a Plane-Wave Basis Set. *Comput. Mater. Sci.* **1996**, *6*, 15.
- (34) Blöchl, P. E. Projector Augmented-Wave Method. *Phys. Rev. B* **1994**, *50*, 17953.
- (35) Perdew, J. P.; Burke, K.; Ernzerhof, M. Generalized Gradient Approximation Made Simple. *Phys. Rev. Lett.* **1996**, *77*, 3865.
- (36) Monkhorst, H. J.; Pack, J. D. Special Points for Brillouin-Zone Integrations. *Phys. Rev. B* **1976**, *13*, 5188.
- (37) Grimme, S.; Ehrlich, S.; Goerigk, L. Effect of the Damping Function in Dispersion Corrected Density Functional Theory. *J. Comput. Chem.* **2011**, *32*, 1456.
- (38) King-Smith, R.; Vanderbilt, D. Theory of Polarization of Crystalline Solids. *Phys. Rev. B* **1993**, *47*, 1651.
- (39) Spaldin, N. A Beginnerundefined Guide to the Modern Theory of Polarization. *J. Solid State Chem.* **2012**, *195*, 2.
- (40) Henkelman, G.; Uberuaga, B. P.; Jónsson, H. A Climbing Image Nudged Elastic Band Method for Finding Saddle Points and Minimum Energy Paths. *J. Chem. Phys.* **2000**, *113*, 9901.
- (41) Paier, J.; Marsman, M.; Hummer, K.; Kresse, G.; Gerber, I. C.; Ángyán, J. G. Screened Hybrid Density Functionals Applied to Solids. *J. Chem. Phys.* **2006**, *124* (15), 154709.
- (42) Perdew, J. P.; Ruzsinszky, A.; Csonka, G. I.; Vydrov, O. A.; Scuseria, G. E.; Constantin, L. A.; Zhou, X.; Burke, K. Restoring the Density-Gradient Expansion for Exchange in Solids and Surfaces. *Phys. Rev. Lett.* **2008**, *100*, 136406.
- (43) Zhou, J.; Lin, J.; Huang, X.; Zhou, Y.; Chen, Y.; Xia, J.; Wang, H.; Xie, Y.; Yu, H.; Lei, J. A Library of Atomically Thin Metal Chalcogenides. *Nature* **2018**, *556*, 355.
- (44) Habib, M. R.; Wang, S.; Wang, W.; Xiao, H.; Obaidulla, S.; Gayen, M. A.; Khan, A. Y.; Chen, H.; Xu, M. Electronic Properties of Polymorphic Two-Dimensional Layered Chromium Disulfide. *Nanoscale* **2019**, *11*, 20123.
- (45) Zhang, C.; Wang, R.; Mishra, H.; Liu, Y. Two-Dimensional Semiconductors with High Intrinsic Carrier Mobility at Room Temperature. *Phys. Rev. Lett.* **2023**, *130*, 087001.
- (46) Zhang, T.; Xu, X.; Huang, B.; Dai, Y.; Ma, Y. 2D Spontaneous Valley Polarization from Inversion Symmetric Single-Layer Lattices. *Npj Comput. Mater.* **2022**, *8* (1), 64.
- (47) Peng, R.; Zhang, T.; He, Z.; Wu, Q.; Dai, Y.; Huang, B.; Ma, Y. Intrinsic Layer-Polarized Anomalous Hall Effect in Bilayer MnBi₂Te₄. *Phys. Rev. B* **2023**, *107*, 085411.
- (48) Zhang, J.; Dai, Y.; Zhang, T. Ferroelectric Metals in Van Der Waals Bilayers. *Appl. Phys. Lett.* **2024**, *124* (25), 252906.
- (49) Li, J.; Yang, X.; Zhang, Z.; Yang, W.; Duan, X.; Duan, X. Towards the Scalable Synthesis of Two-Dimensional Heterostructures and Superlattices Beyond Exfoliation and Restacking. *Nat. Mater.* **2024**, *23*, 1326.
- (50) Zhang, C.; Zhang, Z.; Wu, Z.; Li, X.; Wu, Y.; Kang, J. Modulation of Polarization in Sliding Ferroelectrics by Introducing Intrinsic Electric Fields. *J. Phys. Chem. Lett.* **2024**, *15*, 8049.

- (51) Cheng, X.; Xu, S.; Liu, C.; Cui, Y.; Ouyang, W.; Jia, F.; Wu, W.; Ren, W. Ferroelectric and Negative Piezoelectric Properties in Oxyhydroxide Monolayers γ -XOOH (X = Al, Ga, and In). *Appl. Phys. Lett.* **2023**, *123* (7), 072904.
- (52) Gao, W.; Chelikowsky, J. R. Prediction of Intrinsic Ferroelectricity and Large Piezoelectricity in Monolayer Arsenic Chalcogenides. *Nano Lett.* **2020**, *20*, 8346.
- (53) Tripathy, N.; Sarkar, A. D. Insights into the Origin of Multiferroicity and Large In-Plane Piezoelectricity in AlXY (X = S, Se; Y = Cl, Br, I) Monolayers. *Phys. Rev. B* **2024**, *109* (12), 125414.
- (54) Hu, H.; Sun, Y.; Chai, M.; Xie, D.; Ma, J.; Zhu, H. Room-Temperature Out-of-Plane and In-Plane Ferroelectricity of Two-Dimensional β -InSe Nanoflakes. *Appl. Phys. Lett.* **2019**, *114* (25), 252903.
- (55) Sui, F.; Li, H.; Qi, R.; Jin, M.; Lv, Z.; Wu, M.; Liu, X.; Zheng, Y.; Liu, B.; Ge, R.; Wu, Y.-N. Atomic-Level Polarization Reversal in Sliding Ferroelectric Semiconductors. *Nat. Commun.* **2024**, *15* (1), 3799.
- (56) Zhang, Y.; Peng, Y.; Liu, F.; Li, K.; Zhong, N.; Liu, Y.; Hao, Y.; Han, G. Interface-Roughness Effect on Polarization Switching and Reliability Performance of Doped-HfO₂ Capacitors. *IEEE Trans. Electron Devices* **2023**, *70*, 3788.
- (57) Heron, J. T.; Bosse, J. L.; He, Q.; Gao, Y.; Trassin, M.; Ye, L.; Clarkson, J. D.; Wang, C.; Liu, J.; Salahuddin, S. Deterministic Switching of Ferromagnetism at Room Temperature Using an Electric Field. *Nature* **2014**, *516*, 370.
- (58) Liu, S.; Grinberg, I.; Rappe, A. M. Intrinsic Ferroelectric Switching from First Principles. *Nature* **2016**, *534*, 360.
- (59) Bian, R.; Cao, G.; Pan, E.; Liu, Q.; Li, Z.; Liang, L.; Wu, Q.; Ang, L. K.; Li, W.; Zhao, X. High-Performance Sliding Ferroelectric Transistor Based on Schottky Barrier Tuning. *Nano Lett.* **2023**, *23*, 4595.
- (60) Sun, W.; Wang, W.; Hu, R.; Yang, C.; Huang, S.; Li, X.; Cheng, Z. Ultra-High-Density Ferroelectric Array Formed by Sliding Ferroelectric Moiré Superlattices. *Nano Lett.* **2023**, *23*, 11280.
- (61) Yu, M.; Hilse, M.; Zhang, Q.; Liu, Y.; Wang, Z.; Law, S. Review of Nanolayered Post-Transition Metal Monochalcogenides: Synthesis, Properties, and Applications. *ACS Appl. Nano Mater.* **2024**, *7*, 28008.
- (62) Bian, R.; He, R.; Pan, E.; Li, Z.; Cao, G.; Meng, P.; Chen, J.; Liu, Q.; Zhong, Z.; Li, W. Developing Fatigue-Resistant Ferroelectrics Using Interlayer Sliding Switching. *Science* **2024**, *385*, 57.
- (63) Yasuda, K.; Zalys-Geller, E.; Wang, X.; Bennett, D.; Cheema, S.; Watanabe, K.; Taniguchi, T.; Kaxiras, E.; Jarillo-Herrero, P.; Ashoori, R. Ultrafast High-Endurance Memory Based on Sliding Ferroelectrics. *Science* **2024**, *385*, 53.